

# Pressure drops for droplet flows in microfluidic channels

Brian J Adzima and Sachin S Velankar

Department of Chemical Engineering, University of Pittsburgh, Pittsburgh, PA 15261, USA

E-mail: [velankar@pitt.edu](mailto:velankar@pitt.edu)

Received 9 March 2006, in final form 17 May 2006

Published 22 June 2006

Online at [stacks.iop.org/JMM/16/1504](http://stacks.iop.org/JMM/16/1504)

## Abstract

Designing on-chip microfluidic pumps requires that the dependence of pressure drop across the device on the fluid flow rate be known. This relationship can be complicated for the case of two-phase droplet type flows. We characterized the flow-pressure relationship for the single-file flow of water drops in oil in microfluidic channels of rectangular cross sections. The pressure for such droplet flows was always larger—sometimes over 50% larger—than that for corresponding single-phase flows of the continuous phase. This is in spite of the fact that the water drops had a substantially lower viscosity than the continuous phase oil. The excess pressure was found to correlate reasonably well with the size of the drops relative to the size of the channels. This correlation for the excess pressure, as well as a correlation presented here for the size of drops in microchannels, should provide convenient guidelines in designing microfluidic devices for two-phase flows.

## 1. Introduction

The microfluidic lab on a chip approach calls for increasing levels of functionality on a single platform. In recent years, this has included measuring numerous properties (concentration, pH and viscosity), achieving mixing, reaction, separation, dispersion of drops and numerous other operations in microfluidic devices [1, 2]. A particularly challenging issue is integrating fluid pumps on microfluidic chips. Various approaches of achieving on-chip pumping have been reviewed in a recent article [3]. These include electroosmotic flows [4, 5], electrowetting [6, 7], thermocapillary motion [8] and motion of optically trapped microparticles [9]. Newer principles of implementing micropumps are reported frequently [10–14]. As integrated pumps become more common, the issue of pump ‘sizing’ will become important: how much fluid can a given pump deliver or, conversely, the design problem, how much pressure must a pump be capable of developing for a specific application?

For a single-phase flow of a Newtonian fluid, this issue can be resolved in a straightforward fashion: the low Reynolds number of most microfluidic flows allows an exact solution of the Stokes equation. Thus the pressure drop versus flow rate relationship of the device (henceforth called the flow-pressure characteristic) may be calculated accurately even for complex

flow geometries. One may then design a pump that can develop the pressure necessary to achieve the desired flow rate. In contrast, for two-phase flows, it is more difficult to calculate the pressure-flow characteristics *a priori* because the wetting properties of the channel are likely to influence the pressure-flow characteristics. The situation is especially complicated when the two-phase flow involves drops, since the capillary pressure associated with the drops is also likely to affect the pressure-flow characteristics.

The purpose of this paper is to quantify the pressure-flow characteristics for two-phase droplet flow for the simplest microfluidic geometry of a straight channel of rectangular cross section. We seek to address the following questions. Does the pressure-flow characteristic differ significantly for single-file droplet flow as compared to a corresponding single-phase flow? If so, can we establish correlations, say in terms of the drop size, or flow rates, or appropriate dimensionless quantities, that may be used as guidelines in designing pumps for specific applications? Beyond these principal issues, we will also present results on sizes of drops and provide design correlations for these quantities.

## 2. Experimental details

Microchannels were made by replicating SU8-on-silicon molds in PDMS (Sylgard 184) using well-established

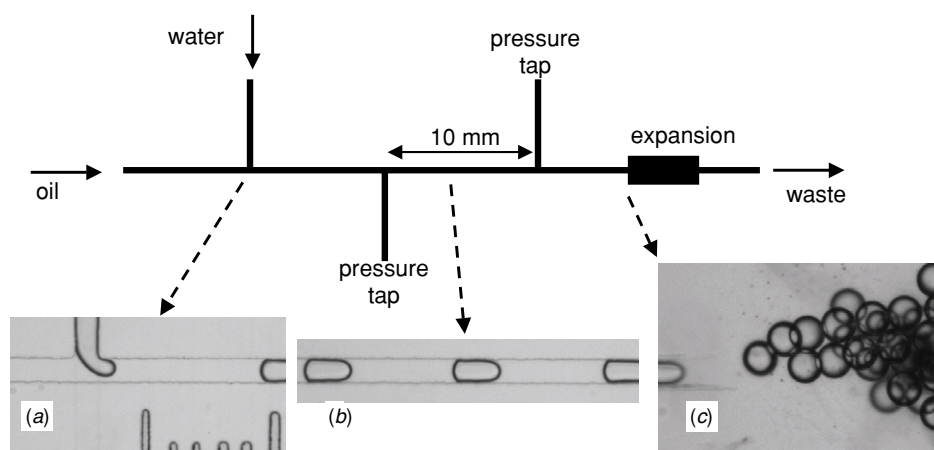


**Figure 1.** Schematic of the device. Three devices were studied with cross-sectional dimensions of the main channel (width  $\times$  depth) being  $105 \times 74$ ,  $200 \times 95$  and  $300 \times 95 \mu\text{m}$ . The water and oil inlets had the same dimensions as the main channel. The pressure taps had widths of  $200 \mu\text{m}$  in all three devices. The section labeled ‘expansion’ was made by taping Scotch tape onto the SU8-on-silicon mold. Hence it has greater depth than the rest of the device. The three photographs are (a) a water drop being formed at the T-junction, (b) a single file of drops in the pressure-measurement section and (c) drops retracting into spheres in the expansion section.

procedures [15]. The PDMS replicas were exposed to plasma treatment using a Harrick scientific plasma cleaner (PDC-32G) at a maximum power setting of 100 W for 30 s. They were then immediately sealed against glass slides. External connections to gas-tight syringes were made using medical grade polyethylene tubing (Intramedic, outer diameter 0.965 mm). Syringes were driven by two programmable syringe pumps. The wettability of the microchannel walls was found to affect the range of flow rates over which drops could be generated, the size of the drops, and their behavior in the microchannels (elaborated further at the end of this paper). Therefore, the following procedure was used to ensure consistent wetting properties: the microfluidic devices, after connecting the tubing, but before passing any fluid through the device, were treated again in the plasma cleaner for 30 s. Immediately after this treatment, a  $\sim 0.05 \text{ mol l}^{-1}$  solution of octadecyltrichlorosilane (OTS) in hexadecane was pumped into the channels, allowed to sit for 5 min, and then flushed out with pure hexadecane. Extensive past literature indicates that the OTS can silanize the plasma-treated PDMS surface, resulting in grafting of the octadecyl chains onto the surface. The resulting coating of OTS ensured consistent hydrophobicity of the walls of the device and reproducible behavior of drops in the channels.

Experiments were conducted using hexadecane with 1 wt% of surfactant Span 80 as the continuous phase and water as the drop phase. This hexadecane/surfactant mixture is henceforth called ‘oil’ in this paper. Hexadecane was found to swell the PDMS, with an equilibrium swelling estimated at about 14 wt%. However, this swelling is relatively rapid and was expected to equilibrate before experiments were initiated. The swelling also introduces an approximately 5% error in the channel dimensions; however, only the unswollen dimensions are used in all calculations. None of the conclusions are significantly affected by this uncertainty in channel dimensions.

The device geometry is shown in figure 1. The flow of oil sheared off drops of water at a T-junction as shown in figure 1(a) [16]. The water drops are convected down the length of the channel (figure 1(b)). A close examination of

the receding front of the drops suggests that the drops do not make direct contact with the walls, but instead, a thin wetting layer of oil remains in contact with the walls at all times, as also reported by others [16–18]. This is also consistent with our own measurements of the wettability of flat PDMS sheets coated with OTS using a similar procedure as above (5 min dipping into a  $0.05 \text{ mol l}^{-1}$  solution of OTS). The coated sheets were found to be fully hydrophobic (the oil/water contact angle was  $180^\circ$ ), consistent with the presence of a wetting oil layer on the walls at all times.

The pressure drop was measured using differential pressure sensors (Honeywell 26PC series) connected across pressure taps. The output of the pressure sensor was recorded at 1000 Hz on a computer using a Labview data acquisition system. This measured pressure drop corresponds to several drops (7–30, see below) that are present in the 10 mm test section between the pressure taps. One may expect that as each drop passes a pressure tap, the pressure may fluctuate [19]. However, in our experiments, this fluctuation was not evident, and only the average pressure drop for the two-phase droplet flow could be measured.

Just before exiting the device, the drops were allowed to expand into a larger ‘cavity’ that was both deeper as well as wider than the microchannels (figure 1(c)). This allowed the drops to relax into spherical shapes, thus allowing their diameter (designated  $2R_d$ ) to be measured accurately. The single-file flow of drops in the pressure-measurement section was also imaged directly (figure 1(b)), and the spacing between the drops was measured from such images. The number of drops in the test section was calculated from the inter-drop spacing and was found to range from 7 to 30, depending on flow rates. All imaging was performed using an inverted microscope (Olympus CKX41) and a digital camera (Basler A302fs).

Since pressure drop measurements are the primary motivation for this research, these measurements were validated using single-phase flow of various fluids through glass capillaries. These validation tests were conducted exactly like the actual experiments, except that the microfluidic devices were replaced by round capillaries of known diameter.

The pressure drop across the capillaries was verified to be proportional to the flow rate, and the viscosities calculated from the pressure versus flow rate curves were in excellent agreement with values measured in a rheometer. During these tests, we found that it was critical to minimize the length of Tygon tubing used to connect the pressure sensor to the device. Any more than a few mm of Tygon tubing caused excessively long transients in the pressure drop upon changing flow rate, presumably due to compliance of the tubing. (The Tygon tubing could not be eliminated altogether since the ports of the pressure sensors, which are ~6.4 mm in diameter, are best sealed by soft, flexible tubing.)

### 3. Results

There are two quantities of interest: the pressure drop and the drop size, and we will consider each of these below. Furthermore, we will non-dimensionalize each of these quantities and attempt to establish correlations in terms of the controlled parameters. Such correlations would prove useful in designing microfluidic devices for handling droplet flow.

#### 3.1. Drop sizes

Figure 2 shows the diameter,  $2R_d$ , of drops generated in channels with the three different dimensions noted in the figure. As mentioned in the previous section, the diameter was measured after the drops had retracted into spheres in the cavity (figure 1(c)). Each series of points corresponds to varying the flow rate of water  $Q_w$  at a constant oil flow rate  $Q_o$ . Two trends are immediately evident: (1) at a given  $Q_o$ , drops are larger as  $Q_w$  increases, and (2) lowering  $Q_o$  increases the drop size substantially. These trends are similar to those noted previously by other researchers [16, 20–22]. Furthermore, a comparison of the various channels shows that the drop size increases with channel dimensions.

We now seek a correlation that collapses all the data of figure 2 into a single master curve that has the form

$$R_d = f(Q_w, Q_o, \mu_w, \mu_o, \sigma, \text{effective channel dimension}) \quad (1)$$

where  $\mu_w$  and  $\mu_o$  are the viscosities of the water and oil, respectively, and  $\sigma$  is the equilibrium interfacial tension (~0.0036 N m) between water and hexadecane/surfactant. The drop size must scale with the dimensions of the channel at the T-junction. Since the channels are not circular, but rectangular, some definition of an effective channel dimension is necessary. We adopt the area-equivalent radius (which gives the same area as the rectangular channel) as the effective dimension of the microchannel. It is defined as

$$\pi R^2 = A \quad (2)$$

where  $A$  is the area of the rectangular cross section of the channel. This value of  $R$  will be used to make the drop radius,  $R_d$ , dimensionless.

The remaining variables ( $Q_w, Q_o, \mu_w, \mu_o, \sigma$ ) can be combined into the following dimensionless parameters:

$$p = \frac{\mu_w}{\mu_o} \quad \phi = \frac{Q_w}{Q_{\text{total}}} \quad Ca = \frac{V\mu_o}{\sigma} = \frac{Q_{\text{total}}\mu_o}{A\sigma} \quad (3)$$

where  $p$  is the viscosity ratio,  $\phi$  is the fractional flow rate of the drop phase,  $Ca$  is the capillary number and  $V$  is the mean

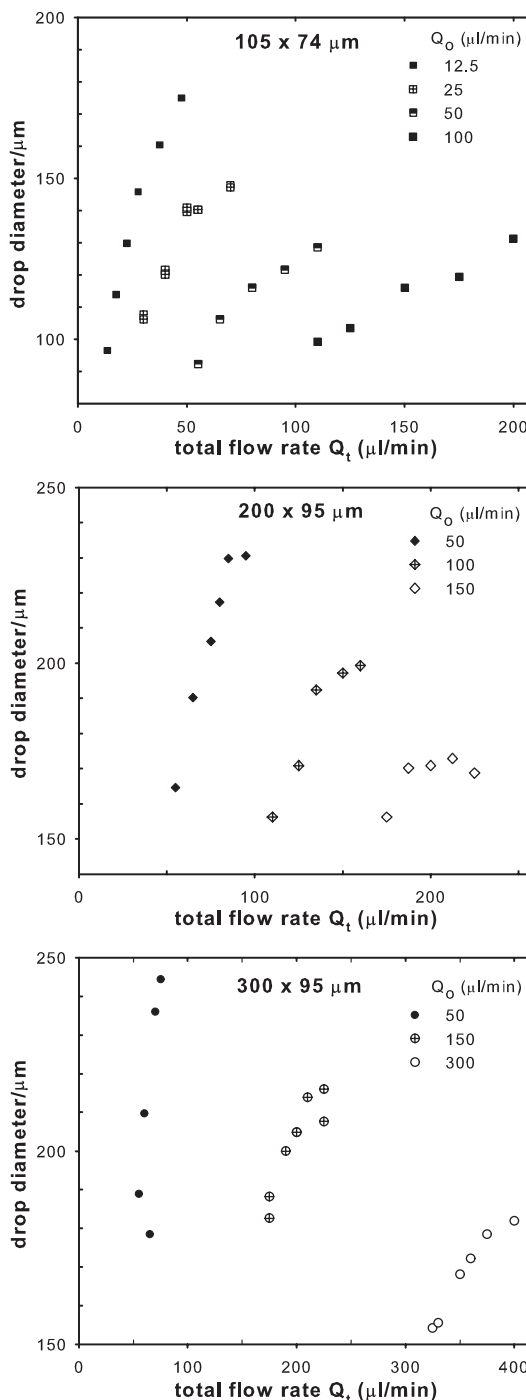


Figure 2. Drop diameters in the three different microfluidic devices. The cross-sectional dimensions of each device are given at the top of each figure.

velocity in the channel:

$$V = \frac{Q_{\text{total}}}{A} = \frac{Q_w + Q_o}{A} \quad (4)$$

In summary, dimensional analysis suggests seeking a correlation of the form

$$\frac{R_d}{R} = f(p, \phi, Ca). \quad (5)$$

The viscosity ratio  $p$  was kept constant for all the experiments here. Furthermore, for a given channel,  $Ca$  is

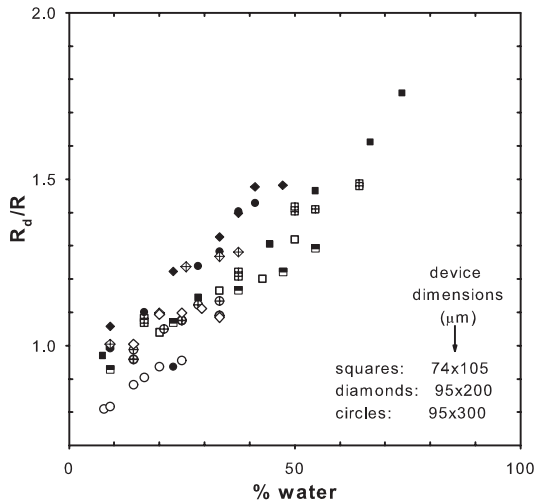


**Figure 3.** Correlation for dimensionless drop radius in terms of the relative flow rate of water.

proportional to  $Q_{\text{total}}$  itself, thus, simply rescaling in terms of  $Ca$  will not collapse the data at the different oil flow rates onto a single master curve. This leaves the volume fraction of water as the last remaining parameter. A plot of dimensionless drop radius versus  $\phi$  (figure 3) does indeed collapse the data for each of the three channels into relatively narrow bands. Remarkably, in spite of the different aspect ratios of these channels, the scaled data for all three channels are also quite close to each other. This gives confidence that the area-equivalent radius, equation (2), is indeed the appropriate effective dimension for scaling the drop size.

Finally, in a recent article, Garstecki *et al* [17] have derived a relationship for the size of water drops generated by a carrier oil phase at a T-junction:

$$\frac{L}{w} = 1 + \alpha \frac{Q_w}{Q_o} \quad (6)$$

where  $L$  is the length of the drop plug,  $w$  is the width of the microfluidic channel and  $\alpha$  is a coefficient of order 1. Our data were found inconsistent with this scaling, perhaps because the theory applies at low capillary numbers, whereas  $Ca \sim 2$  to 35 for our experiments.

### 3.2. Pressure drop–flow rate relationships

We now turn to the main quantity of interest which motivated this work: pressure drop. Figure 4 shows the pressure-flow characteristics for the three different channels studied.

Considering first the single-phase flow of the continuous phase oil, the pressure-flow characteristic is generally not a straight line as may be expected for rigid channels (and was verified for glass capillaries during the validation tests). Instead, the slope of the pressure versus flow rate curve decreases at higher flow rates, especially for the channel with the highest aspect ratio. Some non-linearity is expected from the compliance of the PDMS walls: as pressure increases, the walls flex slightly, thus increasing the inner dimensions of the channel. Yet, calculations suggest that this mechanism is likely to increase the internal dimensions by only about 1% which is not sufficient to explain the largest deviations

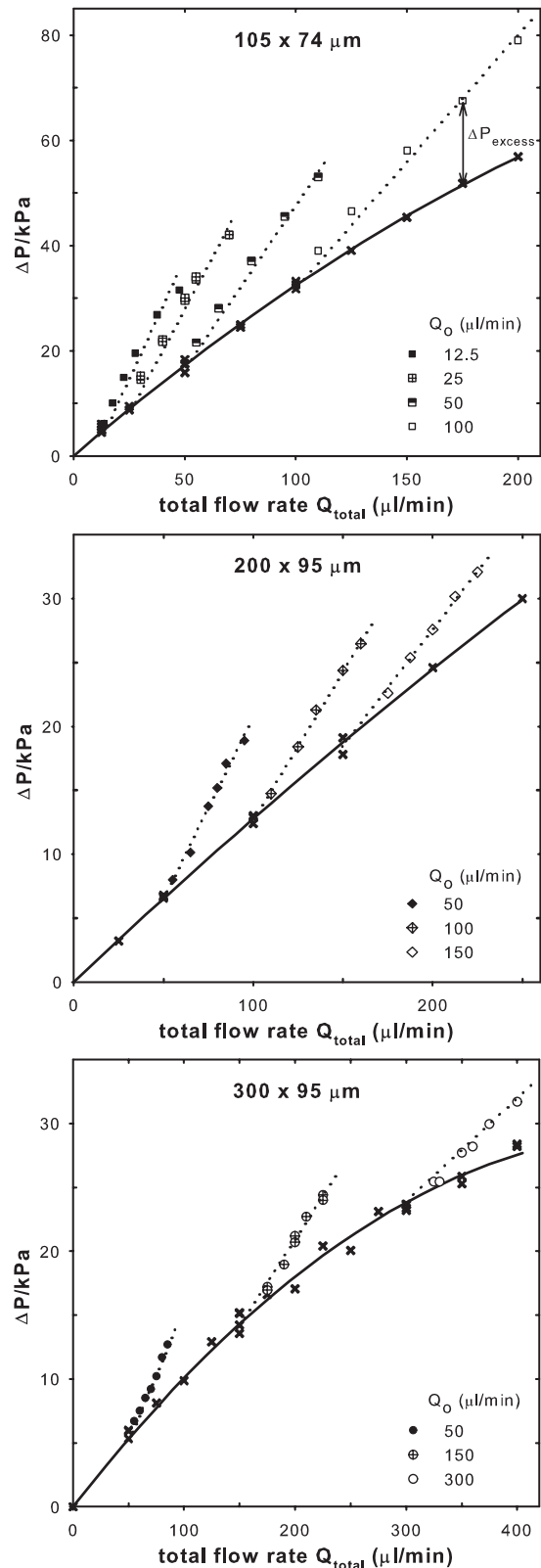


**Figure 4.** Pressure drop for single-phase flow of oil (x) and for two-phase flow of water drops in oil. The solid lines are fits to the data for single phase flow of oil of the form  $\Delta P = aQ_o(1 - bQ_o)$ , where  $a$  and  $b$  are both positive. The dotted lines are guides to the eye; these are drawn such that they intersect the solid line at  $Q_{\text{total}} = Q_o$ . The figure for the  $104 \times 75 \mu\text{m}$  channel shows the excess pressure schematically.

from linearity. We have no adequate explanation for the non-linearity at present.

In preliminary experiments on a few devices, we also measured the pressure-flow characteristic for single-phase flow of water and found that the pressure was about a factor of three lower for water than for oil at the same flow rate. This is consistent with the lower viscosity of water ( $\sim 1$  mPa s) as compared to the surfactant-hexadecane mixture (2.95 mPa s, as measured in a rheometer) [18].

Finally, we consider the pressure-flow characteristics for the single-file flow of water drops carried by the oil phase. Figure 4 shows that at a constant  $Q_o$ , the pressure drop for drop flow increases almost linearly with  $Q_w$ . The principal observation from figure 4 is that the pressure drop for single-file flow of drops always exceeds that for the single-phase flow of the oil at the same *total* flow rate. Thus, we may define the excess pressure (also shown schematically in the top graph of figure 4) as

$$\Delta P_{\text{excess}} = (\Delta P \text{ for droplet flow}) - (\Delta P \text{ for continuous phase flow}). \quad (7)$$

The latter is the pressure drop per unit length if all drops were replaced by the continuous phase. In the present research, this is calculated by simply fitting a low-order polynomial (in this case, the three quadratics shown in figure 4) to the pressure-flow characteristic of the single-phase oil flow.

What is the source of this excess pressure? There may be several possible causes [23]: additional viscous stresses due to a modification of the velocity profile by the drops, capillary pressure of the drops and Marangoni stresses induced by gradients in surfactant concentration at the drop surface. In any case, this excess pressure can be substantial, especially at small  $Q_o$ , e.g. in the  $105 \times 74 \mu\text{m}$  channel, the droplet flow with  $Q_o = 25 \mu\text{l min}^{-1}$  and  $Q_w = 45 \mu\text{l min}^{-1}$  requires  $\sim 80\%$  more pressure than that needed for oil alone with  $Q_o = 70 \mu\text{l min}^{-1}$ . This is especially remarkable considering that the water has a three-fold *lower* viscosity than the oil phase. We therefore conclude that accounting for this excess pressure is critical in designing pumps that are integrated into microfluidic devices.

Accordingly, we seek to develop a design correlation for the excess pressure that would be useful as a tool for sizing microfluidic pumps. For such a correlation, it is essential to make the excess pressure dimensionless. We will do so by two different approaches. The first ‘fluid mechanics’ approach, motivated by past literature on the low- $Re$  motion of drops in round tubes [23], is to use the characteristic viscous stress,  $\mu_o V/R$ , to scale the excess pressure per drop:

$$\frac{\text{Excess pressure per drop}}{\text{Viscous stress}} = \frac{\Delta P^+ R}{\mu_o V} \quad (8)$$

where  $\Delta P^+$  is the excess pressure drop per drop

$$\Delta P^+ = \frac{\Delta P_{\text{excess}}}{\text{Number of drops in the test section}}. \quad (9)$$

The number of drops in the test section (calculated from the drop spacing and the 10 mm length of the test section) ranged from about 7 to 30. The second ‘engineering’ approach is to define:

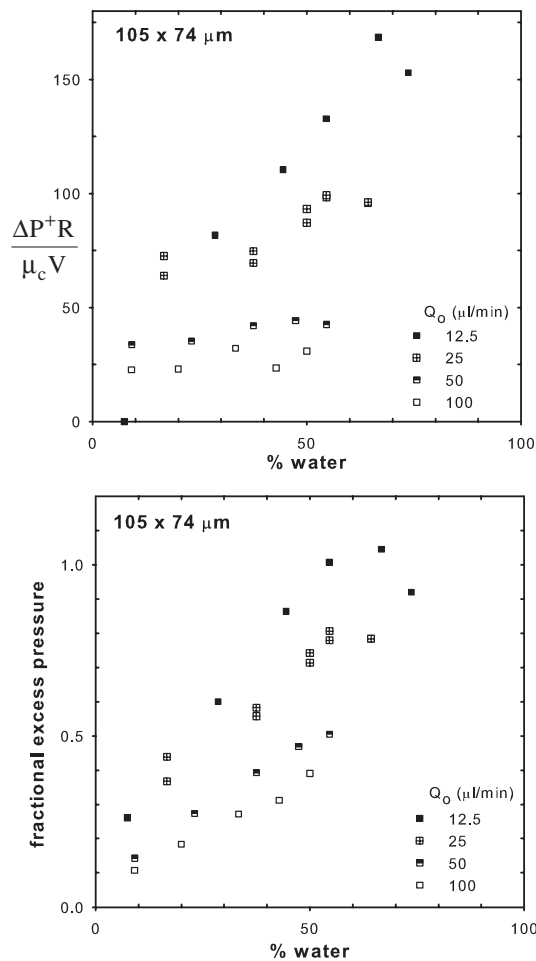


**Figure 5.** Dependence of excess pressure on relative flow rate of water. (a)  $\frac{\Delta P^+ R}{\mu_o V}$  and (b) fractional excess pressure.

Fractional excess pressure

$$= \frac{\Delta P_{\text{excess}}}{\Delta P \text{ for continuous phase flow at the total flow rate}}. \quad (10)$$

Once again, it must be emphasized that the denominator in equation (10) is the pressure drop for single-phase oil flow at the *total* flow rate. The fractional excess quantity is motivated by a practical engineering perspective: obviously, if the fractional excess pressure is small (say 0.1), that excess may be ignored when designing a microfluidic pump, and all calculations may be done on the basis of the total flow rate.

Dimensional analysis suggests that the excess pressure must depend on four dimensionless parameters: the viscosity ratio  $p$ , the dimensionless drop size  $R_d/R$ , the capillary number  $Ca$  and the relative flow rate of water  $\phi$ . As mentioned in section 3.1, since viscosity, interfacial tension and the channel dimensions are all fixed for a given channel,  $Ca$  is proportional to the oil flow rate itself. Thus, plotting the excess pressure in terms of  $Ca$  will not result in a useful correlation. This leaves  $\phi$  and the dimensionless drop size as the only remaining parameters.

Figure 5 shows  $\frac{\Delta P^+ R}{\mu_o V}$  (equation (8)) and the fractional excess pressure (equation (10)) for the  $105 \times 74 \mu\text{m}$

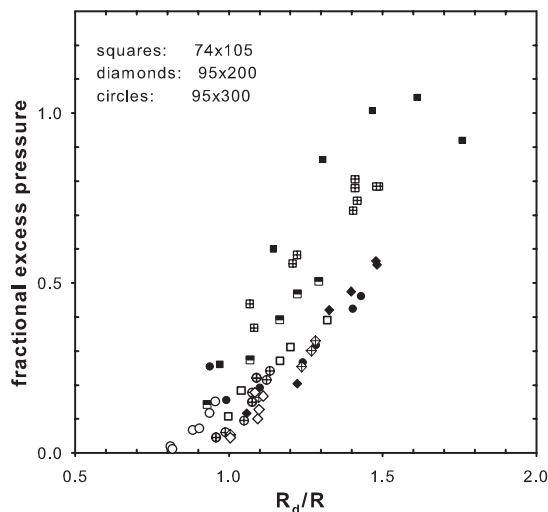


**Figure 6.** Dependence of fractional excess pressure on dimensionless drop size.

channel as a function of  $\phi$ . Both these quantities increase significantly with volume fraction of water; furthermore, they are significantly higher at low flow rates. The same is true for the other two channels (not shown). Theory of drops translating in round tubes suggests that  $\Delta P_{\text{excess}}$  increases significantly with drop size [23]. Figure 3 has already shown that drop size increases sharply as the volume fraction of water increases or as the oil flow rate decreases, thus, figures 5(a) and (b) may be more an indication of the dependence of  $\Delta P_{\text{excess}}$  on drop size rather than the volume fraction *per se*. Indeed, a plot of the fractional excess pressure versus dimensionless drop size (figure 6) does collapse the data into relatively narrow bands for each of the three channels. While the data for the various flow rates and different channels are scattered and do not superpose perfectly, figure 6 may still provide a useful design correlation. Certainly figure 6 offers a convenient rule of thumb: when designing microfluidic devices for drops with size  $R_d < R$ , the excess pressure due to the two-phase nature of the flow may be ignored.

#### 4. Summary and concluding remarks

We have studied the single-file flow of water drops suspended in a hexadecane/surfactant continuous phase oil in microfluidic channels. The microchannels had rectangular cross sections of modest aspect ratios, and the drop sizes were comparable to the cross-sectional dimensions of microchannels. We make the following observations that may prove useful in the design of microfluidic devices to handle droplet flows:

- The size of water drops generated by shearing them off at a T-junction, scaled by the area-equivalent diameter of the microchannels, correlates well with the flow rate of water relative to the total flow rate.
- Single-file flow of water drops in oil can require substantially higher pressure than a corresponding single-phase flow of the oil phase alone. This is despite the fact that the viscosity of water was far *lower* than of the oil phase used here. The excess pressure required for the

two-phase flow increases with the size of the drops. The results show that when designing microfluidic pumps to handle drop flows, the excess pressure may be neglected if the drops are substantially smaller than the cross-sectional dimensions of the microchannels.

Finally we note that all experiments were conducted on channels whose walls were almost completely hydrophobic since they had been coated with a hydrophobic silane. A limited number of experiments were also performed on uncoated devices whose walls were partially wetting towards oil and water. The generation and flow of drops were less reproducible in such uncoated devices. Yet, comparing coated and uncoated channels, two differences were evident: (1) at the same flow rates  $Q_o$  and  $Q_w$ , the uncoated devices generally produced larger drops, and (2) at the same relative drop size  $R_d/R$ , the uncoated channels showed far higher fractional excess pressures than those presented here. We speculate that the moving water/oil contact lines in the uncoated channels are responsible for the latter effect.

#### Acknowledgments

This research was partly funded by an NSF-CAREER award #0448845. The authors thank Professor Barnard, University of Pittsburgh, for the use of his pendant drop apparatus for measuring oil/water interfacial tension. The authors are grateful to Dr Sandy Hu, University of Pittsburgh, for helping with the microfabrication of the devices, and to Mr Todd Crosby for his initial research in this area.

#### References

- [1] Squires T M and Quake S R 2005 Microfluidics: fluid physics at the nanoliter scale *Rev. Mod. Phys.* **77** 977–1026
- [2] Stone H A, Stroock A D and Ajdari A 2004 Engineering flows in small devices: microfluidics toward a lab-on-a-chip *Ann. Rev. Fluid Mech.* **36** 381–411
- [3] Laser D J and Santiago J G 2004 A review of micropumps *J. Micromech. Microeng.* **14** R35–R64
- [4] Lazar I M and Karger B L 2002 Multiple open-channel electroosmotic pumping system for microfluidic sample handling *Anal. Chem.* **74** 6259–68
- [5] Morf W E, Guenat O T and de Rooij N F 2001 Partial electroosmotic pumping in complex capillary systems, Part 1: Principles and general theoretical approach *Sensors Actuators B* **72** 266–72
- [6] Yun K S, Cho I J, Bu J U, Kim C J and Yoon E 2002 A surface-tension driven micropump for low-voltage and low-power operations *J. Microelectromech. Syst.* **11** 454–61
- [7] Satoh W, Loughran M and Suzuki H 2004 Microfluidic transport based on direct electrowetting *J. Appl. Phys.* **96** 835–41
- [8] Darhuber A A and Troian S M 2005 Principles of microfluidic actuation by modulation of surface stresses *Ann. Rev. Fluid Mech.* **37** 425–55
- [9] Terray A, Oakey J and Marr D W M 2002 Microfluidic control using colloidal devices *Science* **296** 1841–4
- [10] Brask A, Goranovic G, Jensen M J and Bruus H 2005 A novel electro-osmotic pump design for nonconducting liquids: Theoretical analysis of flow rate-pressure characteristics and stability *J. Micromech. Microeng.* **15** 883–91
- [11] Pan T R, McDonald S J, Kai E M and Ziaie B 2005 A magnetically driven PDMS micropump with ball check-valves *J. Micromech. Microeng.* **15** 1021–6

- [12] Song W H and Lichtenberg J 2005 Thermo-pneumatic, single-stroke micropump *J. Micromech. Microeng.* **15** 1425–32
- [13] Oh K W, Rong R and Ahn C H 2005 Miniaturization of pinch-type valves and pumps for practical micro total analysis system integration *J. Micromech. Microeng.* **15** 2449–55
- [14] Yin Z Z and Prosperetti A 2005 A microfluidic ‘blinking bubble’ pump *J. Micromech. Microeng.* **15** 643–51
- [15] McDonald J C, Duffy D C, Anderson J R, Chiu D T, Wu H, Schueller O J A and Whitesides G M 2000 Fabrication of microfluidic systems in poly(dimethylsiloxane) *Electrophoresis* **21** 27–40
- [16] Thorsen T, Roberts R W, Arnold F H and Quake S R 2001 Dynamic pattern formation in a vesicle-generating microfluidic device *Phys. Rev. Lett.* **86** 4163–6
- [17] Garstecki P, Fuerstman M J, Stone Howard A and Whitesides G M 2005 Formation of droplets and bubbles in a microfluidic T-junction-scaling and mechanism of break-up *Lab Chip* **6** 437–46
- [18] Link D R, Anna S L, Weitz D A and Stone H A 2004 Geometrically mediated breakup of drops in microfluidic devices *Phys. Rev. Lett.* **92** 054503
- [19] Chio H, Jensen M J, Wang X L, Bruus H and Attinger D 2006 Transient pressure drops of gas bubbles passing through liquid-filled microchannel contractions: an experimental study *J. Micromech. Microeng.* **16** 143–9
- [20] Cygan Z T, Cabral J T, Beers K L and Amis E J 2005 Microfluidic platform for the generation of organic-phase microreactors *Langmuir* **21** 3629–34
- [21] Tice J D, Song H, Lyon A D and Ismagilov R F 2003 Formation of droplets and mixing in multiphase microfluidics at low values of the Reynolds and the capillary numbers *Langmuir* **19** 9127–33
- [22] Nisisako T, Torii T and Higuchi T 2002 Droplet formation in a microchannel network *Lab Chip* **2** 24–6
- [23] Olbricht W L 1996 Pore-scale prototypes of multiphase flow in porous media *Ann. Rev. Fluid Mech.* **28** 187–13